Primordial Gravitational Waves

João Viana - joaoviana@alunos.fc.ul.pt.

May 22nd 2025

1 Introduction

Primordial gravitational waves might have been created shortly after the Big Bang in a strong first-order electroweak phase transition. They were produced by the collision of matter dragged by bubbles of true vacuum, the collisions left only a stochastic background noise of gravitational waves that can be detected in the near future. In this lecture, we are going to take a brief look at each step of the way to calculate the signal strength of these gravitational waves.

It is well known that the SM does not allow for a strong first-order electroweak phase transition, only a second-order phase transition it predicted by the SM. For this reason, this type of calculation is done to scalar extension of the standard model, where such transition can occur.

2 Phase transitions

Using the effective potential we can plot the scalar potential and see where the minima of the potential are, which we need if we want to use perturbative theory. We see that at very high T the potential has a mininum at the origin but at $T = 0$ the minimum is at a different place, breaking $SU(2)_L \times U(1)_Y \to U(1)_Q$.

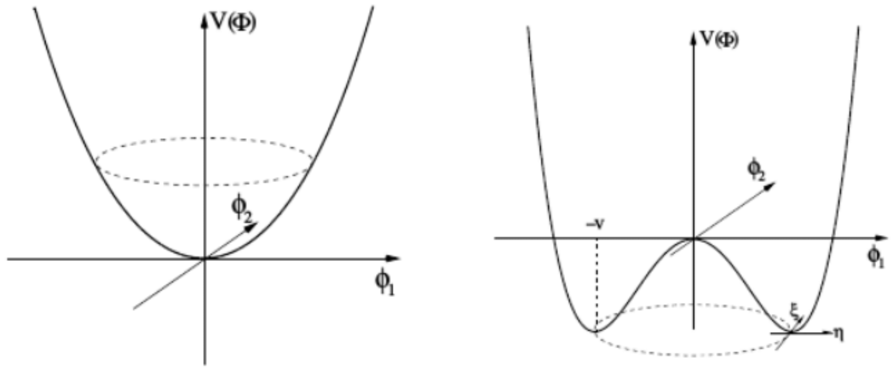

Figure 1: Higgs potential at high temperature (left) and zero temperature (right).

But what happens in the middle? Is the transition smooth with no jumps in the VEVs (2nd order phase transition) or do we change VEVs quickly (1st order phase transition)?

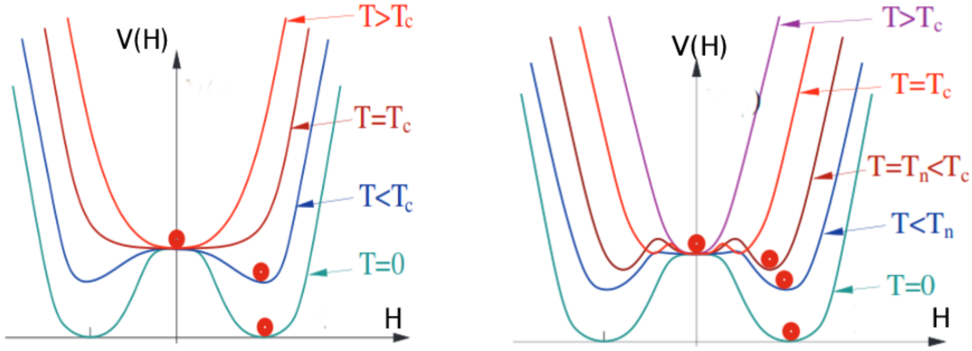

Figure 2: 2nd order phase transition (left) and 1st order phase transition (right)

A first order phase transition would be the most interesting case for us. It fulfils the "out of equilibrium" epoch Sakharov conditions, can induce baryogenesis and primordial gravitational waves. Due to the quantum mechanical nature of the system, a first order phase transition occurs via quantum tunnelling.

3 QFT at finite temperature

The usual QFT formalism assumes that you are working in a vacuum, the same is not true right after the Big Bang when the Universe was super dense and hot. The temperature of the Universe comes by approximating it by a thermodynamical system with internal energy, entropy, pressure and temperature, which can be done at large enough scales (cosmological principle). Due to this fact, we have to consider that all processes occur in a thermal bath with the Universe which motivates us to use the grand canonical ensemble to describe its properties, as both energy and particles can be exchanged with the thermal bath. We will define the grand ensemble density operator as

$$\hat{\rho} = e^{-\beta(\hat{H}-\mu_i \hat{N}_i)}\,, \tag{1}$$

where $\beta = \frac{1}{T}$ (inverse of temperature T, we use natural units, $c = k_b = \hbar = 1$), $\hat{H}$ is the hamiltonian operator, $\hat{N}_i$ is the number operator of particle i and μ_i is the chemical potential of particle i. The quantum partition function is given by

$$Z = \mathrm{Tr}\,\hat{\rho}, \quad \text{with}\,\mathrm{Tr}(\ldots) = \langle n| \ldots |n\rangle\,. \tag{2}$$

As always, grand canonical ensemble averages are given by

$$\langle \mathcal{O} \rangle = \frac{\mathrm{Tr}\,\mathcal{O}\hat{\rho}}{Z}\,, \tag{3}$$

and, as a consequence, Green functions are also affected since

$$G^C(x_1, \ldots, x_n) \equiv \langle T_c \phi(x_1) \ldots \phi(x_n) \rangle \tag{4}$$

In the end, we are going to have temperature-dependent Feynman rules given, in imaginary time formalism, by [1]

$$\begin{aligned}
\text{Boson propagator} &: \frac{i}{p^2 - m^2}; p^\mu = \left[2ni\pi\beta^{-1}, \vec{p}\right]\,, \\
\text{Fermion propagator} &: \frac{i}{\gamma \cdot p - m}; p^\mu = \left[(2n+1)i\pi\beta^{-1}, \vec{p}\right]\,, \\
\text{Loop integral} &: \frac{i}{\beta} \sum_{n=-\infty}^{\infty} \int \frac{d^3p}{(2\pi)^3}\,, \\
\text{Vertex function} &: -i\beta(2\pi)^3 \delta\omega_i \delta^{(3)}\left(\sum_i \vec{p}_i\right)\,,
\end{aligned} \tag{5}$$

where $\omega_n = 2n\pi\beta^{-1}$ (bosons) and $\omega_n = (2n+1)\pi\beta^{-1}$ (fermions) are the Matsubara frequencies.

4 Effective potential

4.1 Historical example

The effective potential serves as a way to simplify calculations by either reducing number of particles or diagrams. An exemple of an effective potential is Fermi's theory of the β decay, which he though to be a quartic interaction but instead is a s-channel mediated by a W boson.

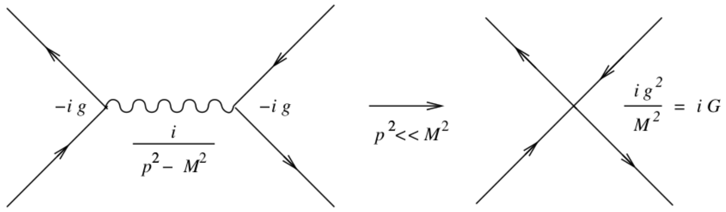

In the limit of low centre of mass energy, the W boson propagator appears to be simply $1/m_W^2$. In this example, Fermi unintentionally integrated out the W boson.

4.2 Finite temperature effective potential

The same can be done to include higher order diagrams in a tree level potential, this is precisely what Coleman and Weinberg did in in 1970s [2] where they computed all 1-loop diagrams and constructed an effective potential which made calculation of NLO effects much easier (as well as loop induced symmetry breaking).

Our goal is to construct an effective potential that approximates the behaviour of temperature in interactions. The complete potential is given by

$$V_{\text{eff}}(T) = V_0 + V_{\text{CW}}^{(1)} + \Delta V(T) + V_{\text{ct}}\,, \tag{6}$$

where V_0 is the tree level potential, $V_{\text{CW}}^{(1)}$ is the Coleman-Weinberg potential, V_{ct} is the counterterm potential and $\Delta V(T)$ are the finite-temperature 1-loop corrections. The Coleman-Weinberg potential is given by

$$V_{\text{CW}}^{(1)} = \frac{1}{64\pi^2} \sum_a n_a m_a^4(h,\phi) \left[\log \frac{m_a^2(h,\phi)}{\mu^2} - C_a \right], \tag{7}$$

where n_a counts the number of degrees of freedom and for a particle of spin s_a is given by

$$n_a = (-1)^{2s_a} Q_a N_a (2s_a + 1),$$

where N_a stands for the number of colours and $Q_a = 1, 2$ for neutral/charged particles. $m_a(h,\phi)$ correspond to (tree-level) field-dependent masses. One-loop thermal corrections are given by [1]

$$\Delta V(T) = \frac{T^4}{2\pi^2} \left\{ \sum_b n_b J_B \left[\frac{m_i^2(\phi_\alpha)}{T^2} \right] - \sum_f n_f J_F \left[\frac{m_i^2(\phi_\alpha)}{T^2} \right] \right\}, \tag{8}$$

where J_B and J_F are the thermal integrals for bosons and fermions, respectively, provided by

$$J_{B/F}(y^2) = \int_0^\infty dx\, x^2 \log\left(1 \mp \exp\left[-\sqrt{x^2 + y^2}\right]\right)\,. \tag{9}$$

The counterterm Lagrangian V_{ct} is calculated by imposing that, at $T = 0$, the Coleman-Weinberg potential should not change the tree level VEVs, masses and mixing angles. It is given by

$$\left\langle \frac{\partial V_{\text{ct}}}{\partial h_i} \right\rangle = \left\langle -\frac{\partial V^{(1)}_{\text{CW}}}{\partial h_i} \right\rangle , \qquad \left\langle \frac{\partial^2 V_{\text{ct}}}{\partial h_i \partial h_j} \right\rangle = \left\langle -\frac{\partial^2 V^{(1)}_{\text{CW}}}{\partial h_i \partial h_j} \right\rangle . \tag{10}$$

At finite temperature, the so-called daisy diagrams induce debye masses that have to be included in the potential, the thermal masses are given by

$$m^2_\alpha(T) = m^2_\alpha + c_\alpha T^2 , \tag{11}$$

where the c_α coefficients can be calculated as follows

$$c_\alpha = \frac{\delta^2 \Delta V^{(1)}(T, \phi_h, \phi_\sigma)|_{\text{L.O.}}}{\delta \phi^2_\alpha} . \tag{12}$$

There are two ways to include these correction in the effective potential

- Parwani : Use $m^2_i(T)$ in the Coleman-Weinberg and 1-loop thermal corrections.
- Arnold-Espinosa : $V_{\text{eff}}(T) \to V_{\text{eff}}(T) - \frac{T}{12\pi} \sum_i (m^2_i(T))^{\frac{3}{2}} - (m^2_i(T=0))^{\frac{3}{2}}$

5 Vacuum decay

5.1 Tunneling rate

The probability amplitude for remaining in the false vacuum after time T is:

$$\begin{aligned} \langle \phi_{\text{false}} | e^{-HT} | \phi_{\text{false}} \rangle &= \sum_n \langle \phi_{\text{false}} | e^{-HT} | n \rangle \langle n | \phi_{\text{false}} \rangle & (13) \\ &= \sum_n e^{-E_n T} \langle \phi_{\text{false}} | n \rangle \langle n | \phi_{\text{false}} \rangle & (14) \\ &\simeq e^{-E_0 T} \left| \langle n | \phi_{\text{false}} \rangle \right|^2 & (15) \end{aligned}$$

where $|n\rangle$ are the hamiltonian eigenstates with $H |n\rangle = E_n |n\rangle$.

The decay rate is related to the imaginary time of the energy as

$$\Gamma = -2 \, \text{Im} \, E_0 \tag{16}$$

On the other hand, we can look at this from the path integral formalism. The probability amplitude for remaining in the false vacuum after time T is:

$$\langle \phi_{\text{false}} | e^{-HT} | \phi_{\text{false}} \rangle = \int_{\phi(0)=\phi_{\text{false}}}^{\phi(T)=\phi_{\text{false}}} \mathcal{D}\phi(t) \, e^{-S_E[\phi]},$$

where $S_E[\phi]$ is the Euclidean action:

$$S_E[\phi] = \int_{-T/2}^{T/2} dt \left[\frac{1}{2} \left(\frac{d\phi}{dt} \right)^2 + V(\phi) \right].$$

The integral is dominated by the classical solution $\overline{\phi}$ (see steepest descent method) which can be calculated from the classical equations of motion. The path integral is then given by

$$\langle \phi_{\text{false}} | e^{-HT} | \phi_{\text{false}} \rangle \approx e^{-S_E[\overline{\phi}]} \left[\int_{\phi(0)=\phi_{\text{false}}}^{\phi(T)=\phi_{\text{false}}} \mathcal{D}\phi(t)\, e^{-\delta^2 S_E[\phi]} \right] \tag{17}$$

where

$$\delta^2 S_{\mathrm{E}}[\overline{\phi}] = \frac{1}{2} \int \left[\delta\phi \left(-\frac{\mathrm{d}^2}{\mathrm{d}\tau^2} + V''(\overline{\phi}) \right) \delta\phi \right] \mathrm{d}\tau \tag{18}$$

are the quadratic fluctuations of the action, remember that for the classical path the first action variation vanishes, i.e. $\delta S_{\mathrm{E}}[\overline{\phi}] = 0$. After also considering the contribution from n bounces and summing everything. We are left with the following results for the path integral

$$\langle \phi_{\text{false}} | e^{-HT} | \phi_{\text{false}} \rangle = \int_{\phi(0)=\phi_{\text{false}}}^{\phi(T)=\phi_{\text{false}}} \mathcal{D}\phi(t)\, e^{-S_E[\phi]} = (\det M_0)^{-1/2} e^{Ae^{-B}\, T} \tag{19}$$

where M_0 is the operator of the second variation of the action.

The decay rate per volume $\Gamma = \#$ transitions$/(V \cdot t)$ of the false vacuum to the true vacuum can be parameterized as

$$\Gamma \equiv \Gamma(\text{False Vacuum} \to \text{True Vacuum}) = Ae^{-B} \tag{20}$$

where $B = S_E[\overline{\phi}]$ is the Euclidian action of the classical path, A are the quantum correction coming from the second variation of the action.

5.2 $O(4)-$symmetric actions

The equation of motion for the field, in imaginary time, is given by

$$\left(\frac{\partial^2}{\partial\tau^2} + \nabla^2 \right) \phi = V'(\phi) \tag{21}$$

with the boundary conditions

$$\lim_{\tau \to \pm\infty} \phi(\tau, \vec{x}) = \phi_f \quad \text{(False vacuum)}\,, \tag{22}$$

$$\frac{\partial\phi}{\partial\tau}(0, \vec{x}) = 0\,. \tag{23}$$

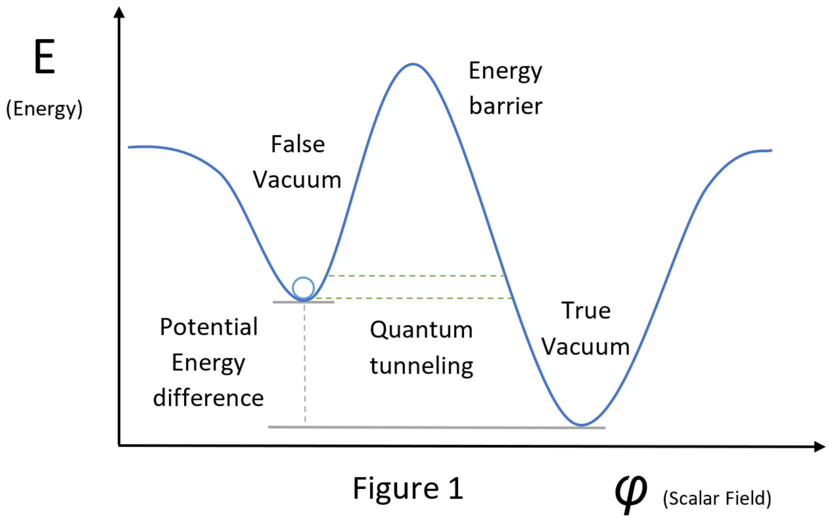

Figure 1

The action can be calculated as

$$S_4 = \int d\tau \int dx^3 \left(\frac{1}{2} \left(\frac{\partial \phi}{\partial \tau} \right)^2 + \frac{1}{2} (\nabla \phi)^2 + V(\phi) \right) , \tag{24}$$

to be finite, we must meet the following conditions

$$\lim_{|\vec{x}| \to \infty} \phi(\tau, \vec{x}) = \phi_f \quad \text{(False vacuum)} , \tag{25}$$

$$V(\phi_f) = 0 . \tag{26}$$

The first condition basically states at far away from the transition the false vacuum remains undisturbed. Coleman proved that the smallest action is given is $O(4)$-symmetric so we are motivated to assume that the field must only depend on a single variable ρ defined as

$$\rho = \sqrt{\tau^2 + \vec{x}^2}. \tag{27}$$

The equation of motion are then

$$\frac{d^2\phi}{d\rho^2} + \frac{3}{\rho}\frac{d\phi}{d\rho} = V'(\phi) \tag{28}$$

and the action is given by

$$S_4 = 2\pi^2 \int_0^\infty \rho^3 \left[\frac{1}{2} \left(\frac{d\phi}{d\rho} \right)^2 + V(\phi) \right] . \tag{29}$$

Notice that Eq.(32) can be interpreted as the motion of a particle in an inverted potential $-V(\phi)$ with a drag term. If we compute the variation of energy for $\rho > 0$ we find

$$\frac{d}{d\rho}\left[\frac{1}{2}\left(\frac{d\phi}{d\rho}\right)^2 - V(\phi)\right] = -\frac{3}{\rho}\left(\frac{d\phi}{d\rho}\right)^2 \leq 0. \tag{30}$$

which means that, in the particle analogy, energy is lost at we take ρ from 0 to ∞.

5.3 Proof that there is always a bounce solution

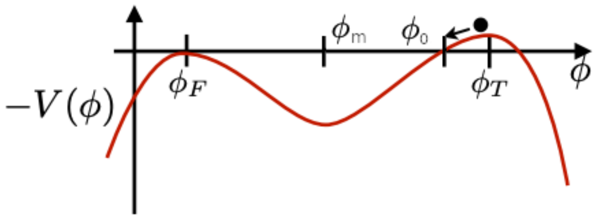

In this section, we are going to show that the quantum tunneling from a false vacuum to true vacuum is always possible, although the decay rate can be arbitrarily low.

If we interpret ρ as time, then Eq.(32) can describe the movement of a particle dropped somewhere rest at $\rho = 0$ which ends up in ϕ_f when $\rho \to \infty$ (which is a local maximum of the inverted potential). Looking at the inverted plot, its clear that if we drop the particle at the left of ϕ_0 and to the right of ϕ_m the particle will never have enough energy to reach ϕ_f, this is called an undershoot. If we let the particle go very close to ϕ_t then, since it is near a stationary point, the particle will spend a very long time there that allows us to neglect the drag term $\propto \frac{1}{\rho}$, in this case the particle will have more than enough energy to reach ϕ_f, this is called an overshoot. Therefore, in the middle there must a be a position ϕ_s where you drop the particle and ends up at ϕ_f at $\rho \to \infty$.

In this analogy, if we take ρ from $-\infty$ to ∞ the particle starts near ϕ_f for an infinitely long time then, near $\rho = 0$, the particle goes to a position ϕ_s and then back to ϕ_f taking, again, an infinitely long time. Due to this behaviour, Eq.(32) is called the bounce equation and the the $O(4)$-symmetric solution is called the bounce solution.

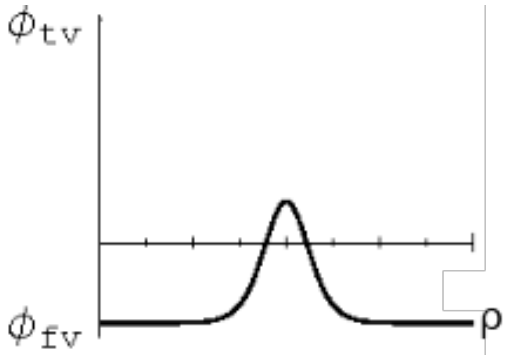

Figure 3: Plot of the bounce solution as a function of ρ.

5.4 Bounce solution at $T = 0$

This allows us to calculate the tunnelling rate of our current VEV. The standard model is in a meta-stable configuration.

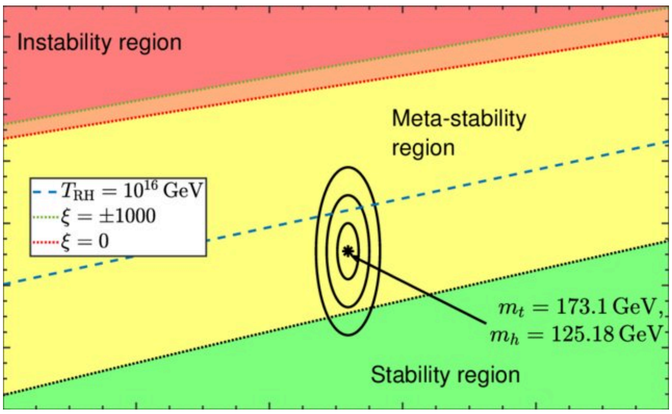

Figure 4: Plot of the bounce solution as a function of ρ.

Concerning! If you think the SM is all there is.

A similar check can be done for BSMs (beyond Standard Model) by requiring that the electroweak (EW) minimum is either the global minimum (so it does not decay) or that it is long-lived compared to the age of the Universe.

5.5 Bounce solution at finite T

It was shown [3] that at finite temperature, the bounce solution is $O(3)$-symmetric and the integration over imaginary time should spit out a $1/\beta$. Then one should use

$$S_4 \to \frac{S_3}{T}. \tag{31}$$

in the expression for the vacuum decay. The action has the following equation of motion

$$\frac{d^2\phi}{d\rho^2} + \frac{2}{\rho}\frac{d\phi}{d\rho} = V'(\phi)\,, \tag{32}$$

and can be calculated as

$$S_3 = 4\pi \int_0^\infty \rho^2 \left[\frac{1}{2}\left(\frac{d\phi}{d\rho}\right)^2 + V(\phi)\right]\,. \tag{33}$$

5.6 GWs on the Standard model

The SM predicts a second-order transition for its EWPT at around $T_c \approx 160$ GeV and no GW signal is expected. But we have motivations to look for beyond SM physics

- Neutrino masses
- Dark matter
- Missing $\mathcal{CP}$ violation

which might change the scalar sector, i.e. we can have 1st order EWPT.

6 Gravitational Waves

6.1 Einstein Field Equations

The Einstein field equations (EFEs) are given by:

$$G_{\mu\nu} = \frac{8\pi G}{c^4} T_{\mu\nu}, \tag{34}$$

where $G_{\mu\nu} = R_{\mu\nu} - \frac{1}{2} g_{\mu\nu} R$ is the Einstein tensor, $R_{\mu\nu}$ is the Ricci tensor, R is the Ricci scalar, $T_{\mu\nu}$ is the energy-momentum tensor, G is Newton's gravitational constant, and c is the speed of light.

6.2 Linearized Gravity

To study gravitational waves, we consider a small perturbation $h_{\mu\nu}$ on flat Minkowski space:

$$g_{\mu\nu} = \eta_{\mu\nu} + h_{\mu\nu}, \quad \text{with } |h_{\mu\nu}| \ll 1, \tag{35}$$

where $\eta_{\mu\nu} = \text{diag}(-1, +1, +1, +1)$ is the Minkowski metric.

We raise and lower indices using $\eta_{\mu\nu}$, and keep only terms linear in $h_{\mu\nu}$.

6.3 Linearized Ricci Tensor

The Christoffel symbols to first order in $h_{\mu\nu}$ are:

$$\Gamma^{\lambda}_{\mu\nu} = \frac{1}{2}\eta^{\lambda\rho}\left(\partial_\mu h_{\nu\rho} + \partial_\nu h_{\mu\rho} - \partial_\rho h_{\mu\nu}\right). \tag{36}$$

The linearized Ricci tensor is:

$$R_{\mu\nu} = \partial_\lambda \Gamma^{\lambda}_{\mu\nu} - \partial_\nu \Gamma^{\lambda}_{\mu\lambda}. \tag{37}$$

Plugging in the linearized Christoffel symbols:

$$R_{\mu\nu} = \frac{1}{2}\left(\partial_\lambda\partial_\mu h^{\lambda}_{\nu} + \partial_\lambda\partial_\nu h^{\lambda}_{\mu} - \Box h_{\mu\nu} - \partial_\mu\partial_\nu h\right), \tag{38}$$

where $h = h^{\lambda}_{\lambda}$, and $\Box = \eta^{\rho\sigma}\partial_\rho\partial_\sigma$ is the d'Alembertian operator.

6.4 Linearized Einstein Tensor

The Ricci scalar is:

$$R = \eta^{\mu\nu}R_{\mu\nu}. \tag{39}$$

Then the linearized Einstein tensor becomes:

$$G_{\mu\nu} = R_{\mu\nu} - \frac{1}{2}\eta_{\mu\nu}R. \tag{40}$$

6.5 Gauge Choice: Lorenz Gauge

We define the trace-reversed perturbation:

$$\bar{h}_{\mu\nu} = h_{\mu\nu} - \frac{1}{2}\eta_{\mu\nu}h. \tag{41}$$

Imposing the Lorenz gauge condition:

$$\partial^\mu \bar{h}_{\mu\nu} = 0, \tag{42}$$

simplifies the field equations.

6.6 Wave Equation for Gravitational Waves

In vacuum ($T_{\mu\nu} = 0$), the linearized Einstein equations reduce to:

$$\Box \bar{h}_{\mu\nu} = 0. \tag{43}$$

This is a wave equation, indicating that the perturbations $\bar{h}_{\mu\nu}$ propagate at the speed of light. These are gravitational waves.

6.7 Plane Wave Solutions

A general solution is a plane wave:

$$\bar{h}_{\mu\nu}(x) = \mathrm{Re}\left\{A_{\mu\nu}e^{ik_\lambda x^\lambda}\right\}, \quad k^\mu k_\mu = 0, \tag{44}$$

where $A_{\mu\nu}$ is a constant amplitude tensor, and k^μ is a null wave vector (i.e., the wave propagates at the speed of light).

6.8 Transverse-Traceless (TT) Gauge

Further gauge freedom allows us to impose the TT gauge, where:

$$\bar{h}_{0\mu} = 0, \quad \partial^i \bar{h}_{ij} = 0, \quad \bar{h}^i_i = 0. \tag{45}$$

In this gauge, gravitational waves have only two physical degrees of freedom, commonly called the "plus" and "cross" polarizations. Their effects are given in fig.5.

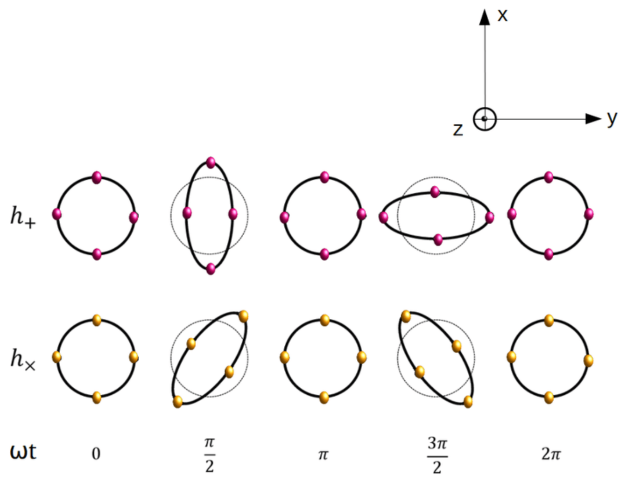

Figure 5: Effect of a GW wave passing through free-falling test masses. There are two polarizations, commonly called the "plus" and "cross".

7 Stochastic Gravitational Wave Background

Now we can join everything. At very high temperature the Universe is in a symmetric vacuum with all VEVs being equal to zero. As the temperature drops the potential will change its shape and different minimum might appear. If these minima have a lower energy than the symmetric (false) vacuum then a transition can occur via quantum tunnelling creating bubbles of true vacuum in a sea of false vacuum. The true vacuum bubbles will expand creating pressure in the highly dense Universe and dragging matter alongside it. The main source of gravitational waves is the collision of matter that is dragged alongside the bubble walls. The goal of this section is to find out when the decay rate is high enough for all this stuff to happen.

7.1 Important temperatures

We are going to start by defining some relevant temperatures.

- **Critical Temperature** - T_c - The potential has two degenerate minima and, consequently, the transition from the false vacuum to the true vacuum begins via quantum tunnelling.

- **Nucleation Temperature** - T_n - There is one bubble nucleated per cosmological horizon. T_n is the solutions of

$$\int_{t_c}^{t_n} \Gamma(T)\, V_H(t)\, dt = \int_{T_n}^{T_c} \frac{dT}{T} \frac{\Gamma(T)}{H(T)^4} = \int_{T_n}^{T_c} \frac{dT}{T} \Big(\frac{2\zeta M_{\rm Pl}}{T}\Big)^4 e^{-\hat{S}_3/T} = 1\,, \tag{46}$$

where $\zeta = 3 \cdot 10^{-3}$ and $M_{\rm Pl}$ is the Planck mass. There is an alternative definition for T_n. It is the temperature at which the tunnelling decay rate matches the Hubble rate

$$\frac{\Gamma(T_n)}{H^4(T_n)} = 1 \tag{47}$$

which can be further approximated, in a crude way, as

$$\frac{\hat{S}_3(T_n)}{T_n} \sim 140\,. \tag{48}$$

- **Percolation Temperature** - T_* - Temperature at which at least 34% of the false vacuum has tunnelled into the true vacuum or, equivalently, the probability of finding a point still in the false vacuum is 70%. This condition imposes that at the percolation temperature there is a large connected structure of true vacuum that spans the whole Universe, and that is stable and cannot collapse back to the false vacuum. This large structure is known as the *percolating cluster*. The probability of finding a point in the false vacuum is given by :

$$P(T) = e^{-I(T)}, \qquad\qquad I(T) = \frac{4\pi v_b^3}{3} \int_T^{T_c} \frac{\Gamma(T')dT'}{T'^4 H(T')} \left(\int_T^{T'} \frac{d\tilde{T}}{H(\tilde{T})} \right)^3 \tag{49}$$

To find the percolation temperature one has to solve $I(T_*) = 0.34$ or, equivalently, $P(T_*) = 0.7$.

7.2 Characterizing GWs

To compute the spectrum of the GWs we have to make use of fits generated from numerical simulations. These fits usually depend on a set of thermodynamical quantities which are

1. Latent heat

The strength of the phase transition, conventionally denoted as α, is related to the latent heat released in the FOPT at the bubble percolation temperature T_*. It is defined as

$$\alpha = \frac{1}{\rho_\gamma}\Big[V_i - V_f - \frac{T_*}{4}\Big(\frac{\partial V_i}{\partial T} - \frac{\partial V_f}{\partial T}\Big)\Big] \tag{50}$$

where $V_i \equiv V_{\rm eff}(\phi^i_{h,\sigma}; T_*)$ is the value of the effective potential at the false vacuum and $V_f \equiv V_{\rm eff}(\phi^f_{h,\sigma}; T_*)$ is the value of the effective potential at the true vacuum. And ρ_γ is the energy density of a radiation-dominated Universe written as a function of the effective number of relativistic degrees of freedom, $g_* \simeq 106.75$ for the standard model. It is given by

$$\rho_\gamma = g_* \frac{\pi^2}{30} T_*^4 \tag{51}$$

2. Inverse time scale

The second important characteristic of the FOPT is the inverse time-scale of the phase transition denoted as β divided by the Hubble parameter H, such that

$$\frac{\beta}{H} = T_* \, \frac{d}{dT}\left(\frac{\hat{S}_3(T)}{T}\right)\Bigg|_{T_*} . \tag{52}$$

The inverse time scale quantifies how long does the transitions last and, consequently, the sizes of the bubble at the time of collision.

3. Bubble wall velocity

The bubble wall velocity is currently very difficult to calculate for a general model so it is usually assumed to be a fraction of the speed of light.

4. Transition temperature

The temperature at which most of the bubbles collide, which is then imprinted into the GW spectrum. Usually, we assume the transition temperature to coincide with the percolation temperature.

7.3 Can we detect them?

It is very important to know whether a GW is considered to be *strong* and can be detected.

A good rule of thumb is the difference of the VEVs between true and false vacuum at the transition temperature. For a strong gravitational wave we need

$$\frac{\Delta v_i}{T_*} > 1 \tag{53}$$

for each field i that acquires a VEV. For baryogenesis we need

$$\sqrt{\sum_i \left(\frac{\Delta v_i}{T_*}\right)^2} > 1 \tag{54}$$

for each field i that couples with the electroweak symmetry for the sphalerons to be efficiently suppressed.

The most important measure of the strength is the signal-to-noise ratio which quantifies the ability of some experiment with sensibility $\Omega_{\text{Sens}}(f)$ to detect a gravitational wave with amplitude $\Omega_{\text{GW}}(f)$ integrated over a period of time $\mathcal{T}$. It is defined as

$$\text{SNR} = \sqrt{\mathcal{T} \int_{f_{\min}}^{f_{\max}} \mathrm{d}f \left[\frac{h^2\Omega_{\text{GW}}(f)}{h^2\Omega_{\text{Sens}}(f)}\right]^2} . \tag{55}$$

LISA is expected to go live in ~ 15 years so most works compute the SNR at LISA.

It is important to illustrate the relations between all these parameters. We plot β/H as a function of α for some standard model scalar extension (CxSM). We also draw the SNR at LISA that show where the strongest GWs are.

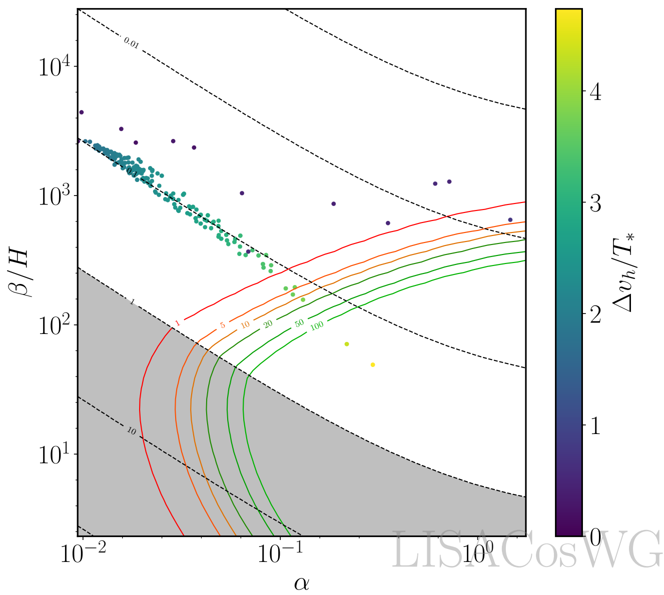

Notice that an higher α means an higher SNR ratio, which makes sense because there is more energy between the false and true vacuum that then can be used to fuel the production of gravitational waves. For the inverse time scale β/H it seems that there is a sweet spot between 10 and 100 where we can have stronger gravitational waves (with higher SNR) with a rather low release of energy. This happens because, if β/H is high then the transition of the whole Universe from the false vacuum to the true vacuum occurs over a large period of time, which means that a lower number of bubbles dominate the transition, low number of bubbles = low number of bubble wall collisions = weak GW signal. Now consider the opposite scenario, if β/H is low then the transition occurs very quickly which means that we had a lot of bubble percolating the Universe into the true vacuum, this means that average bubble size was low. What causes the gravitational waves is the matter that is dragged alongside the bubble walls, if the bubble are small at percolation it means that low quantities of matter were being dragged when the collisions happened, hence creating a weak GW signal.

7.4 Sources of GWs

There are three major sources of GW produced by a strong first-order phase transition. We will neglect the latter.

7.4.1 Sound waves/sock waves

Usually, it is the largest source of gravitational waves. After a vacuum bubble is created, it is energetically viable for the bubble to expand rapidly. As the bubble moves through the cosmic fluid, interactions will drag the fluid alongside the bubble wall. This induces bulk fluid motion, forming a velocity profile in the plasma that travels with the bubble wall. These coherent fluid motions generate sound waves in the plasma, which persist after the bubbles collide. These sound waves are a major contributor to the stochastic gravitational wave background from a first-order EWPT.

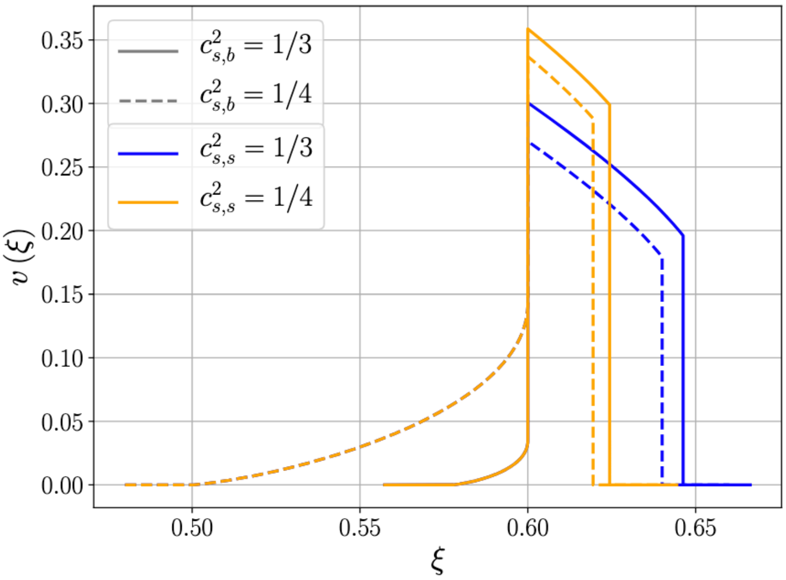

Figure 6: Velocity profile. Hybrid deflagration mode. $v_w = 0.6$

7.4.2 Turbulence

During a strongly first-order electroweak phase transition, expanding bubbles of the broken phase collide and inject energy into the surrounding plasma. These collisions can generate chaotic, turbulent flows in the plasma, especially if nonlinear instabilities develop. The resulting turbulence produces anisotropic stress that sources gravitational waves. Although the gravitational wave signal from turbulence is generally weaker than that from sound waves, it can persist for longer and contribute significantly to the overall spectrum.

7.4.3 Bubble collision

In a strongly first-order electroweak phase transition, bubbles of the new vacuum phase nucleate and expand rapidly. When these bubbles collide, the energy stored in their walls is released violently. These collisions generate anisotropic stress in spacetime, which can produce gravitational waves. This source is usually much weaker than the others (except for supercooled transitions) so it is usually ignored.

7.5 LISA

The SNR curves present in the last plot belong to the predicted sensitivity of an upcoming experiment named LISA over an acquisition period of 3 years. It is going to be an interferometer that uses three satellites arranged in a equilateral triangle with an arm size of around $2.5 \cdot 10^6$ km, it will be placed at around $5 \cdot 10^7$ km from Earth in the year of 2037 (planned).

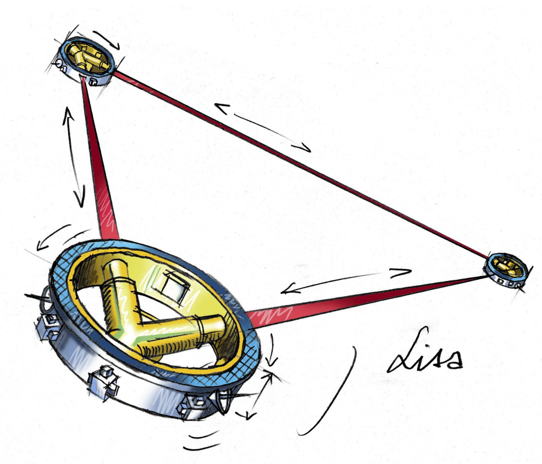

Interferometry works by spliting a beam of light into two, making them travel some set distance and recombining the final beams. Just like the following diagram.

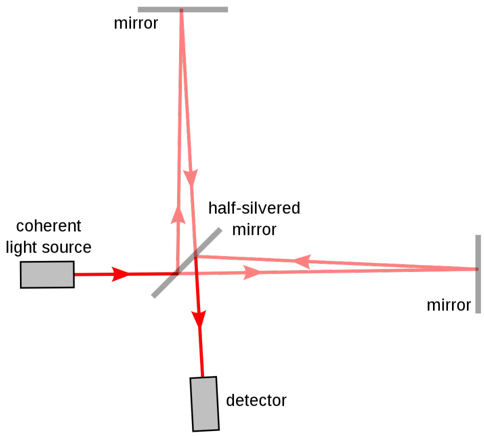

If a gravitational waves passes through the detector, one arm length might change slightly compared with the other one. This effect will shift the phase of one of the beams of light creating interference pattern in the recombined ray. Interferometers much smaller than LISA, such a LIGO and Virgo, have detected gravitational waves from the collision of black holes and/or neutron stars. No primordial gravitational wave was ever detected.

7.6 First indirect GW detection

The Hulse-Taylor pulsar (PSR B1913+16), discovered in 1974, is a pair of neutron stars orbiting each other, one of which is a pulsar. By tracking the timing of the pulsar's radio signals, researchers saw that the orbit was slowly shrinking. This matched the energy loss expected if the system were emitting gravitational waves, just as General Relativity predicted.

It was the first strong evidence that gravitational waves are real. Hulse and Taylor won the 1993 Nobel Prize in Physics for the discovery.

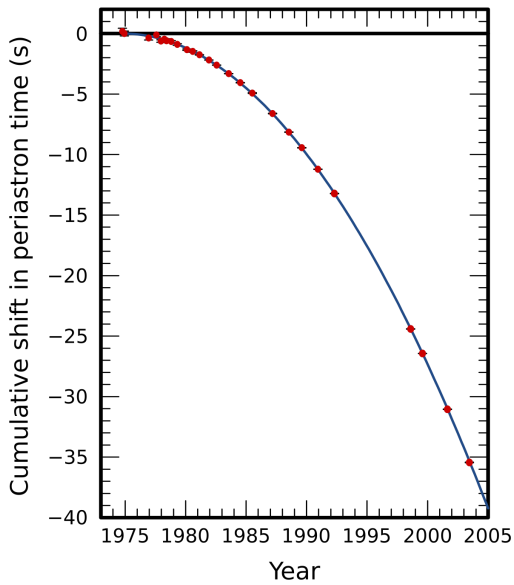

Figure 7: Evidence of orbital decay in PSR B1913+16. The data points indicate the observed change in the time of periastron with date, relative to a system not undergoing decay. The parabola illustrates the theoretically expected change according to general relativity.

7.7 First direct GW detection

The first direct detection of gravitational waves was made on September 14, 2015, by the LIGO detectors. The signal came from the merger of two black holes about 1.3 billion light-years away. This event created ripples in spacetime that LIGO measured as tiny changes in the length of its detectors arms, similar to LISA's mechanism described in sec. 7.5. It was the first time gravitational waves were directly observed.

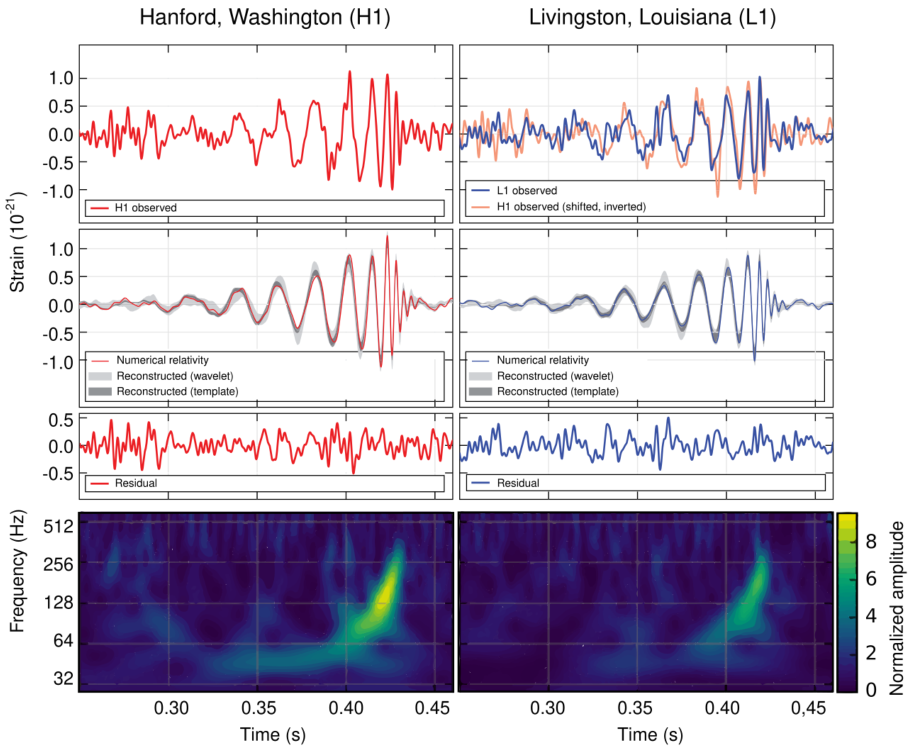

Figure 8: LIGO measurement of the gravitational waves at the Livingston (right) and Hanford (left) detectors, compared with the theoretical predicted values

7.8 Stochastic gravitational wave background signal

The NANOGrav collaboration has found strong evidence for a stochastic gravitational wave background (around 3σ confidence) likely caused by orbiting pairs of supermassive black holes. Using over 15 years of precise timing data from millisecond pulsars, they observed that there is a correlation of the pulse variations as a function of the angular separation ξ_{ab} in the sky. This results seems to be consistent with the GR prediction, more specifically the Hellings-Downs spectrum.

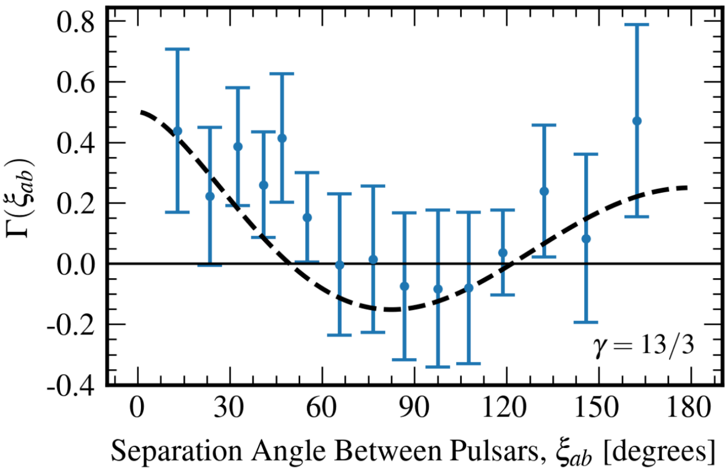

Figure 9: Signal variation correlation as a function of the angular separation in the sky ξ_{ab}.

Unfortunately for us, the usual GWs spectra predicted by strong EWPT are of a much higher frequency so the NANOGrav data cannot be explained by a strong EWPT.

8 Baryogenesis

8.1 Sakharov conditions

In order to generate the baryon asymmetry of the Universe (BAU) we need a models that fulfils all of the Sakharov conditions.

1. Baryon Number Violation

The Standard Model allows for non-perturbative processes that violate both violate baryon (B) and lepton (L) number via electroweak sphalerons, $B - L$ is conserved.

$$\Delta B = \Delta L \neq 0, \quad \Delta(B - L) = 0$$

These sphaleron transitions are efficient only when the $SU_L(2) \times U_Y(1)$ gauge group is unbroken, i.e. zero vacuum expectation value $v = 0$. An example of such transition is

$$u + d \to \bar{d} + 2\bar{s} + \bar{c} + 2\bar{b} + \bar{t} + \bar{\nu}_e + \bar{\nu}_\mu + \bar{\nu}_\tau \tag{56}$$

2. CP Violation

The Standard Model also contains CP violation through the complex phase in the CKM matrix. However, this CP violation is too small in magnitude to explain the observed baryon asymmetry. There are many proposals of models with extended scalar sectors with extra CP-violation in order to explain the BAU. We are particularly interested with spontaneous CP-violation that are associated with complex VEVs such as

$$\langle \Phi_2 \rangle = \frac{1}{\sqrt{2}} \begin{pmatrix} 0 \\ v_2 e^{i\theta} \end{pmatrix} , \tag{57}$$

for the 2-Higgs doublet model (2HDM), a famous SM scalar extension.

3. Departure from Thermal Equilibrium

In the Standard Model, the electroweak phase transition is a 2nd order phase transition rather than a strongly first-order phase transition (for a Higgs mass of 125 GeV), which occurs at around $T_c \simeq 160\,\text{GeV}$. If we want a first order EWPT we must have an extended scalar sector compared to the SM.

8.2 Spontaneous CP-violation (and complex fermion masses)

Let's analyse the consequences of having spontaneous CP-violation. The fermions' Yukawa with Φ_2 is of the form

$$\mathcal{L} \supset -y_i \bar{L} \tilde{\Phi}_2 l_R \tag{58}$$

where L is a doublet with the u-type and d-type left handed quarks, $\tilde{\Phi}_2 = i\sigma_2 \Phi_2$ (same $SU(2)_L$ representation as Φ_2 but symmetric hypercharge) and l_R is the u-type right handed component. For the top quark, the mass is given by

$$m_t = \frac{y_t}{\sqrt{2}} e^{i\theta} v_2 \, , \tag{59}$$

which can be complex if $\theta \neq n\pi$, $n \in \mathbb{Z}$.

At the time of the phase transition, bubbles of true vacuum appear and expand in the early Universe. These bubbles have different VEVs on either side so the *bubble interface* interpolates between the false vacuum and the true vacuum as it expands. From the reference frame of the expanding bubble, there is no time dependence and the VEVs are just functions of some z, the axis perpendicular to the bubble wall[1]. This means that the top mass will also depend on z

$$m_t \equiv m_t(z) = \frac{y_t}{\sqrt{2}} e^{i\theta(z)} v_2(z) \, , \tag{60}$$

similar masses will also appear for other fermions.

[1]It is useful to think about them as planar waves, so there is only dependence on one axis.

8.3 Baryogenesis

As the bubble expands through the cosmic fluid, it will exert some pressure of the particles that penetrate the wall. This force is of the form

$$F = f_{\mathrm{CP}} + \eta f_{\not{\mathrm{CP}}} \tag{61}$$

where $\eta = 1$ for particle and $\eta = -1$ for antiparticles, and $f_{\mathrm{CP}} \gg f_{\not{\mathrm{CP}}}$. This means that particles and antiparticles feel slightly different forces when they go through the bubble wall so they get segregated, i.e. and excess of particles on one side and an excess of antiparticles on the other side. Lets suppose that we have an excess of particles in the true vacuum (inside the bubble wall). Sphalerons processes, which violate B and L, will try to erase this asymmetry but, as they are only efficient on the symmetric phase (outside the bubble) where the $v_{\mathrm{EW}} = 0$, only the antiparticles are converted into particles. We are left with a net excess of particles compared to antiparticles. The mechanism can be seen in fig. 10

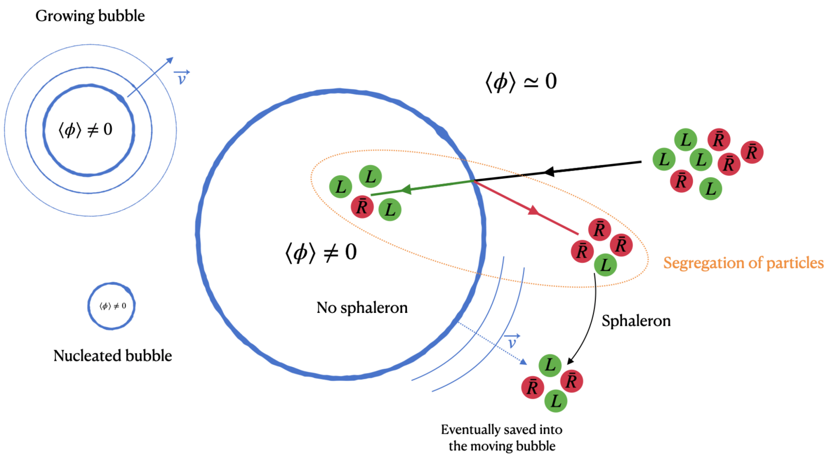

Figure 10: Mechanism that produces an excess number of particles. The bubble wall separates particles and antiparticles, the sphalerons (only efficient in the symmetric vacuum) try to erase that asymmetry by converting antiparticles into particles.

References

[1] Mariano Quiros. Finite temperature field theory and phase transitions, 1999. 3, 4

[2] Sidney Coleman and Erick Weinberg. Radiative corrections as the origin of spontaneous symmetry breaking. *Phys. Rev. D*, 7:1888–1910, Mar 1973. 4

[3] A.D. Linde. Decay of the false vacuum at finite temperature. *Nuclear Physics B*, 216(2):421–445, 1983. 9